Nuclear FAK and Runx1 cooperate to regulate IGFBP3, cell cycle progression and tumor growth

Marta Canel[1,2,*], **Adam Byron**[1,*], **Andrew H. Sims**[1], **Jessy Cartier**[3], **Hitesh Patel**[1], **Margaret C. Frame**[1], **Valerie G. Brunton**[1], **Bryan Serrels**[1,†,‡], and **Alan Serrels**[1,2,†,‡]

[1]Cancer Research UK Edinburgh Centre, Institute of Genetics and Molecular Medicine, University of Edinburgh, Edinburgh EH4 2XR, UK

[2]MRC Centre for Inflammation Research, The Queen's Medical Research Institute, University of Edinburgh, Edinburgh EH16 4TJ, UK

[3]British Heart Foundation Centre for Cardiovascular Science, University of Edinburgh, The Queen's Medical Research Institute, 47 Little France Crescent, Edinburgh EH16 4TJ, UK

Abstract

Nuclear focal adhesion kinase (FAK) is a potentially important regulator of gene expression in cancer, impacting both cellular function and the composition of the surrounding tumor microenvironment. Here we report in a murine model of skin squamous cell carcinoma (SCC) that nuclear FAK regulates Runx1-dependent transcription of insulin-like growth factor binding protein 3 (IGFBP3), and that this regulates SCC cell cycle progression and tumor growth in vivo. Furthermore, we identified a novel molecular complex between FAK and Runx1 in the nucleus of SCC cells and showed that FAK interacted with a number of Runx1 regulatory proteins, including Sin3a and other epigenetic modifiers known to alter Runx1 transcriptional function through post-translational modification. These findings provide important new insights into the role of FAK as a scaffolding protein in molecular complexes that regulate gene transcription.

Keywords

FAK; Runx1; IGFBP3; cell cycle; tumor growth

Introduction

Focal adhesion kinase (FAK) is a non-receptor protein tyrosine kinase that controls diverse cellular functions including cell adhesion, migration, invasion, polarity, proliferation, and survival (1,2). FAK is therefore involved in a number of processes that can impact on the malignant phenotype. Deletion of *fak* in mouse models of cancer has shown a requirement for FAK in tumor formation and progression (3–9). Over-expression of FAK has also been reported in a number of human epithelial tumors (10–12), and it has therefore emerged as a

potential target for cancer therapy, with a number of FAK kinase inhibitors currently being developed (13).

FAK was identified as a protein highly phosphorylated in response to integrin activation and primarily located at cell–extracellular matrix adhesion sites termed focal adhesions (1). Recent reports have also identified that FAK contains nuclear localization signals within the F2 lobe of the four-point-one, ezrin, radixin, moesin (FERM) domain (14) and a nuclear export signal within the kinase domain (15). Therefore, FAK can translocate to the nucleus, where its function remains poorly characterized. Within the nucleus, the FAK FERM domain can bind to the transcription factors p53 and GATA4, resulting in their turnover and inactivation, thereby controlling cell survival and inflammatory signals (14,16). Recently, we reported that nuclear FAK was tethered to chromatin and regulated the expression of chemokines and cytokines, including Ccl5 and TGFβ2, that contribute to establishment of an immuno-suppressive tumor environment through driving elevated intra-tumoral regulatory T-cell numbers (17). Therefore, nuclear FAK protein complexes can act to regulate transcriptional programs important in controlling cellular responses and the composition of the tumor immune environment.

Runt-related transcription factor 1 (Runx1; also known as AML1) is one of a family of three transcription factors (Runx1 - 3) that can either activate or repress transcription depending on the target gene, cell type, and associated co-factors (18,19). It has been shown to have a critical role in hematopoiesis and hematopoietic function (20), and is essential for mammalian development (21). In the context of cancer, Runx1 is best known for its role in acute myeloid leukemia (AML) where it is frequently found mutated (18). In recent years it has also become clear that Runx1 plays an important role in solid epithelial malignancies. For example, Runx1 deficiency impairs mouse skin tumorigenesis (22), while in contrast it acts as a tumor suppressor in the Apc^{Min} mouse model of colorectal carcinogenesis (23). Therefore, it has an important but context dependent function in cancer. Here, we identify a novel molecular complex between FAK and Runx1 in the nucleus of skin squamous cell carcinoma (SCC) cells. We show that nuclear FAK and Runx1 cooperate to regulate expression of IGFBP3, and that IGFBP3 regulates cell cycle progression and tumor growth *in vivo*. Using proteomics and network biology approaches, we identify that nuclear FAK interacts with a number of Runx1 regulatory proteins that can alter Runx1 transcriptional function through post-translational modification. Further, we identify a novel interaction between nuclear FAK and Sin3a, a core component of the Sin3a/HDAC co-repressor complex, and show that Runx1/Sin3a interaction is enhanced in SCC FAK-wt cells. This study provides new insights into the potential mechanisms through which nuclear FAK regulates transcription factor function to control cell behavior.

Materials and Methods

Materials

All antibodies used are listed in Supplementary Materials and Methods. All siRNA was purchased from Dharmacon and shRNA from Open Biosystems.

Cell lines

Cell lines used in this study were generated, authenticated and characterized as previously described (17,24). Cells were pathogen tested in September 2016 using the ImpactIII test (Idex Bioresearch) and were negative for all pathogens. Cell lines are routinely tested for mycoplasma every 2-3 months in-house and have never been found to be mycoplasma positive. Cell lines are cultured for no more than 3 months following freeze thawing. Runx1 or scrambled siRNA was transiently transfected into SCC cells using HiPerFect (Qiagen). Cells were left for 3 days and then immunoblotting or (q)RT-PCR analysis was carried out. Cell lines stably expressing FUCCI, Runx1, or empty-vector shRNA were generated by lentiviral infection and selected in 2 μg/ml puromycin.

Generation of nuclear-targeting FAK mutants

Point mutations were introduced into wild-type FAK in three different combinations, (1) R177A and R178A, (2) K190A and K191A, (3) K216A and K218A, using site-directed mutagenesis as previously described (17). Primer sequences are listed in Supplementary Materials and Methods.

Quantitative RT-PCR

RNA extracts were obtained using an RNeasy kit (Qiagen), following manufacturer's instructions. cDNA was made using a first-strand cDNA synthesis kit (Invitrogen). (q)RT-PCR was performed as previously described (17). Analysis was performed using Rotor-Gene software, and expression relative to B2M was calculated using Excel (Microsoft). Standard PCR was performed using the above conditions but substituting SensiFAST for a 2× PCR master mix. Primers used are listed in Supplementary Materials and Methods.

Nuclear fractionation and total cell lysates

Cells were collected by scraping and low-speed centrifugation (1,000g at 4 °C for 5 min), followed by two washes with ice-cold PBS. Cell pellets were resuspended in buffer A (10 mM KCl, 10 mM HEPES, pH 7.9, 0.5 mM DTT, 1.5 mM MgCl$_2$) and incubated on ice for 15 min. Cells were lysed using a 25G needle and nuclei isolated by centrifugation at 12,000g at 4 °C for 30 sec. The nuclear pellet was washed twice in buffer A and incubated in buffer C (25% (v/v) glycerol, 0.2 mM EDTA, pH 8.0, 0.42 M NaCl, 0.5 mM PMSF, 20 mM HEPES, pH 7.9, 0.5 mM DTT, 1.5 mM MgCl$_2$) at 4 °C for 1 h. Clarification of the nuclear extracts was by high-speed centrifugation (16,000g at 4 °C for 5 min). Alternatively, cells were washed with PBS and lysed in RIPA lysis buffer (50 mM Tris–HCl, pH 7.4, 150 mM sodium chloride, 0.1% SDS and 1% sodium deoxycholate) with inhibitors (Complete Protease Inhibitor Cocktail and PhosSTOP; Roche). Clarification was by high-speed centrifugation (16,000g at 4 °C for 15 min).

Immunoblotting and immunoprecipitation

Cell lysates or cell fractions (10–20 μg protein, as measured by Micro BCA Protein Assay kit (Pierce)) were supplemented with SDS sample buffer (Tris, pH 6.8, 20% glycerol, 5% SDS, β-mercaptoethanol, and bromophenol blue), separated by SDS–PAGE, transferred to nitrocellulose and immunoblotted with specific antibodies at 1:1000 dilution. For

immunoprecipitation experiments, 0.25–1 mg of cell lysate or cell fraction was immunoprecipitated with either 5 μl of mouse Runx1 antibody, 10 μl of agarose-conjugated mouse FAK antibody, 10 μl of agarose-conjugated Myc-tag, or 10 μl of agarose-conjugated control IgG, and immune complexes collected. Beads were washed three times with lysis buffer, once with 0.6 M lithium chloride, and then added to SDS sample buffer.

2D-Gel Electrophoresis

Two-dimensional SDS–polyacrylamide gel electrophoresis was performed using the ZOOM IPGRunner System (ThermoFisher Scientific) according to the manufacturers protocol. Gels were transferred to nitrocellulose membranes, blocked (5 % BSA in TBST) and probed with anti-RUNX1 antibody.

Protein capture arrays

2×10^6 SCC cells were plated onto a 90-mm tissue culture dish and allowed to adhere overnight. Growth medium was removed and replaced with 5 ml of normal growth medium. Cells were cultured for a further 24 hours before conditioned medium was removed and centrifuged at 1000 rpm for 5 minutes. Supernatant was collected and used for analysis. To control for cell number, the 90-mm dish containing SCC cells was lysed in RIPA buffer and protein quantified using a BCA protein assay as described above. This was used to normalize loading of conditioned media onto the protein capture arrays. Secreted protein analysis was performed using mouse angiogenesis protein capture arrays (R & D Systems) according to the manufacturer's protocol. The only modification was the use of a streptavidin DyLight-800 antibody for detection (1:10,000 dilution, Rockland Biochemicals). Image acquisition and analysis was performed using a Licor Imager. Mean spot intensities were calculated from duplicate arrayed spots per cell line. Data were median centered and subjected to unsupervised agglomerative hierarchical clustering on the basis of Pearson correlation computed with a complete-linkage matrix using Cluster 3.0 (C Clustering Library, version 1.50) (25). Clustering results were visualized using Java TreeView (version 1.1.6) (26).

Blood vessel immunostaining

Subcutaneous tumors were surgically excised, placed in an aluminum foil boat, submerged in OCT compound, and snap frozen using a dry ice and methanol bath. OCT-embedded samples were stored long-term at −80°C. For analysis, sections were cut at −20°C onto siliconized microscope slides. For staining, sections were removed from the −20°C freezer, and 50 μl of fixative was applied directly onto the tissue. Sections were incubated for 8 minutes at 4°C and then the fixative removed and the slides allowed to equilibrate to room temperature for approximately 10–20 minutes. Sections were then rehydrated in PBS for 10 minutes. The area of tissue was surrounded with a hydrophobic barrier pen and blocked using 1% horse serum in PBS for 30 minutes at room temperature. Tissue was then incubated with anti-CD31 antibody (BD Biosciences, 1:100 dilution in incubation buffer (1% bovine serum albumin, 1% normal donkey serum, 0.3% Triton X-100, 0.01% sodium azide in PBS)) overnight at 4°C. Slides were washed three times for 15 minutes with PBS, and then incubated with anti-rat Alexa Fluor 594-conjugated secondary antibody (Molecular Probes, ThermoFisher Scientific) diluted at 1:200 in incubation buffer for 1 hour at room

temperature. Slides were washed three times for 15 minutes in PBS and then counter-stained with DAPI for 5 minutes. Slides were washed once for 15 minutes in PBS and mounted in VectaShield anti-fade mounting media (Vectorlabs). Images were acquired using an Olympus FV1000 confocal microscope.

Transcription factor network analysis

Transcription factors were extracted from the DECODE database (Qiagen), selecting the most relevant transcription factors predicted by text mining to bind between 20 kb upstream and 10 kb downstream of the human transcription starting site. The transcription factor Runx1 was used to seed a network of 1000 related proteins using the GeneMANIA plugin (version 3.4.1; human interactions) in Cytoscape (version 3.3.0) (27), onto which proteins specifically isolated in nuclear FAK protein complexes (17) were mapped. The resulting interactome was extracted, and proteins with physical or predicted direct or indirect interactions with Runx1 were analyzed and topological network parameters computed using the NetworkAnalyzer plugin (version 2.7). Networks were clustered using the yFiles Organic algorithm implemented in Cytoscape. Pathway enrichment analysis was performed using the Database for Annotation, Visualization and Integrated Discovery (version 6.8) (28). Pathway terms with Benjamini–Hochberg-corrected P-value < 0.01 were considered significantly overrepresented.

Subcutaneous tumor growth

2.5×10^5 cells were injected subcutaneously into each flank of immune-compromised CD-1 nude mice, and tumor growth measured twice weekly using calipers. Measurements were taken from three mice (each bearing two tumors) for each cell line, and the volume of the tumor (v) was calculated in Excel using the formula $v = 4/3.\pi.r^3$. Data were graphed and statistics calculated using Prism (GraphPad).

In vivo cell cycle analyses

Optical window chambers were implanted onto CD-1 nude mice as described previously (29). All animal work was carried out in compliance with UK Home Office guidelines. 1×10^6 FUCCI-expressing SCC cells were injected into the dermis and at the time of window implantation. 24 hours later, mice were anaesthetized using an isoflurane–oxygen mix and three-dimensional image stacks acquired using an Olympus FV1000 confocal microscope. Image analysis was performed using the spot detection tool in Imaris (Bitplane). The number of green, red, and double-positive nuclei were counted and calculated as a percentage of the total number of cells within the image stack.

Longitudinal *in vivo* imaging of tumor angiogenesis

Optical window chambers were implanted onto CD-1 nude mice as described above. Prior to sealing the window with a coverslip, a tagRFP-expressing tumor fragment (~1 mm in diameter) was placed into the window. To obtain tumor fragments, a donor animal was injected with 2.5×10^5 tagRFP-expressing SCC cells 10 days prior to optical window implantation. Tumors were removed, cut into small pieces using a scalpel, and fluorescence checked using an Olympus OV110 whole-animal imaging system. For longitudinal imaging

of tumor angiogenesis, mice bearing optical windows were anaesthetized using an isoflurane–oxygen mix. Images were acquired 2, 4, 7, and 9 days post-implantation using an Olympus OV110 whole-animal imaging system set to acquire both GFP and RFP signals using the zoom lens set to 1.6× magnification. For image analysis and identification of blood vessels, autofluorescence images acquired using the GFP channel were inverted in ImageJ. The tubness plugin was used to detect blood vessel structures and apply an image mask over these structures. The accuracy of this was checked manually. The vascular density was determined by calculating the percentage of the field of view covered by the vascular image mask. Data were graphed and statistics calculated using Prism.

Results

FAK is required for cell cycle progression and angiogenesis in SCC tumors

We have previously shown using a murine model of skin SCC that depletion of FAK expression can result in immune-mediated tumor regression in syngeneic mice, and a growth delay in immune-deficient mice (17,24). We therefore sought to further dissect the complex role of FAK in regulating SCC tumor growth. We measured tumor growth in CD-1 nude mice following injection of 0.25×10^6 FAK-deficient cells (SCC FAK-/-) and FAK-deficient cells that re-expressed wild type FAK (SCC FAK-wt) at close to endogenous levels. As previously reported, SCC FAK-/- tumors exhibited a growth delay when compared to SCC FAK-wt tumors (24) (Fig. 1a) that was associated with an increased tumor doubling time (Fig. 1b). FAK is a protein that plays a pleiotropic role in regulating cancer development and progression, and we hypothesized that a number of its reported functions, including regulation of proliferation/cell cycle and tumor angiogenesis (1,2,30), may contribute to the observed tumor growth delay in SCC FAK-/- tumors when established on an immune deficient host background. Thus, we set out to use intravital imaging to analyze, in real-time, the cell cycle distribution and kinetics of tumor neo-angiogenesis in SCC FAK-wt and SCC FAK-/- tumors when grown on CD-1 nude mice.

To measure cell cycle distribution in real-time, SCC FAK-wt and SCC FAK-/- cells expressing the fluorescent ubiquitination-based cell-cycle indicator (FUCCI) reporter (31) were implanted via intra-dermal injection under dorsal-skinfold imaging windows. The FUCCI probe is based on the differential proteolysis of geminin and cdt1 at specific phases of the cell cycle, allowing differential profiling of cells at G_1 (red), G_1/S (yellow), and $S/G_2/M$ (green) phases. Images of FUCCI-expressing SCC FAK-wt and SCC FAK-/- tumors revealed an increased number of red fluorescent cells in SCC FAK-/- tumors (Fig. 1c). Analysis of the proportion of red, yellow, and green nuclei from three-dimensional image stacks acquired 24 hours after tumor cell implantation identified a specific delay in the G_1 phase of the cell cycle in SCC FAK-/- tumor cells (Fig. 1d).

FAK, expressed in cancer cells, has been reported to influence tumor angiogenesis through regulating the expression of vascular endothelial growth factor (VEGF) (30). To ascertain whether defective tumor neo-angiogenesis may also be occurring in SCC FAK-/- tumors, we performed longitudinal imaging of tagRFP-labeled SCC FAK-wt and SCC FAK-/- tumors under dorsal-skinfold windows. Using acquisition parameters similar to those required to image green fluorescent protein (GFP), we acquired images of tissue autofluorescence, in

which blood vessels appear as dark non-fluorescent structures that can be readily visualized. Longitudinal imaging of neo-angiogenesis revealed a significant decrease in vascular density in SCC FAK-/- tumors when compared to SCC FAK-wt tumors (Figs. 1e and 1f). Thus, SCC FAK-/- tumors exhibit defective cell cycle progression and neo-angiogenesis that may contribute to defective tumor growth in CD-1 nude mice.

FAK negatively regulates transcription of IGFBP3

We and others have previously identified that FAK can regulate the expression of secreted proteins that have the potential to act in both an autocrine and paracrine manner to influence cancer cell behavior and the surrounding tumor microenvironment (17,32,33). To investigate whether FAK-dependent regulation of secreted factors in SCC cancer cells could influence cell cycle progression and tumor angiogenesis, we screened for secreted factors implicated in both processes using protein capture arrays. Analysis of 53 secreted factors revealed both positive and negative regulation as a consequence of FAK expression (Fig. 2a and Supplementary Fig. 1). Applying a four-fold cutoff for differential regulation, we identified IGFBP3 as the most highly upregulated protein in SCC FAK-/- conditioned medium, while PDGF-AA, PDGF-AB/BB, FGF-1, and MMP-3 were the most highly upregulated proteins identified in SCC FAK-wt conditioned medium. Using these findings, we focused on IGFBP3, a protein belonging to the family of insulin-like growth factor binding proteins (IGFBPs), as this factor has previously been reported to negatively regulate both cell cycle progression (34,35) and angiogenesis (36–38). Western blot analysis of conditioned media confirmed an upregulation of IGFBP3 in SCC FAK-/- conditioned samples (Fig. 2b), and q(RT)-PCR identified similar regulation of *Igfbp3* gene transcript levels (Fig. 2c). Thus, we conclude that FAK negatively regulates the transcription of *Igfbp3*, leading to reduced levels of extracellular secreted IGFBP3 protein.

IGFBP3 is a member of a family of six proteins, IGFBP1–6 (39). However, only antibody capture pairs specific for IGFBP1, 2, and 3 were present on the protein capture arrays used. Therefore, we sought to determine whether FAK regulated the expression of other IGFBP family members. Employing sequence-specific primers designed for each of the six IGFBPs, we used PCR to screen for expression in cDNA libraries prepared from SCC FAK-wt and SCC FAK-/- cells (Fig. 2d). Aside from *Igfbp3*, only expression of *Igfbp4* and *Igfbp6* could be detected following 20 cycles of PCR. All primer sets were confirmed to produce single products of the correct size using cDNA prepared from mouse liver (Supplementary Fig. 2). (q)RT-PCR analysis of *Igfbp4* expression revealed no differential regulation (Fig. 2e), whereas *Igfbp6* expression was observed to exhibit a small but significant decrease in SCC FAK-/- cells when compared to SCC FAK-wt (Fig. 2f). Therefore, IGFBP3 was the only IGFBP family member to be negatively regulated in response to FAK expression.

FAK kinase activity is not required for regulation of IGFBP3

There has been considerable interest in targeting FAK function as a cancer therapy, and a number of small molecule FAK kinase inhibitors are now in early-phase clinical development (13). To determine the role of FAKs kinase activity in regulation of IGFBP3, we tested IGFBP3 protein expression using an SCC FAK-/- cell line in which a FAK kinase-deficient mutant (FAK-kd) had been re-expressed to levels comparable with SCC FAK-wt

cells. Anti-IGFBP3 western blotting from conditioned media revealed that IGFBP3 expression in SCC FAK-kd cells was similar to that observed in SCC FAK-wt cells (Fig. 2g), implying that FAK-dependent regulation of IGFBP3 expression was independent of FAK kinase activity.

IGFBP3 regulates cell cycle progression but not angiogenesis to influence tumor growth

To determine whether increased IGFBP3 expression in SCC FAK-/- cells contributed to the defective growth of SCC FAK-/- tumors, we generated SCC FAK-/- cells with a stable knockdown of IGFBP3 using shRNA (Fig. 3a). Analysis of subcutaneous tumor growth showed that knock-down of IGFBP3 in SCC FAK-/- cells partially restored tumor growth *in vivo* (Fig. 3b), resulting in an average tumor volume of approximately double the size when compared to SCC FAK-/- tumors on day 12. Using intravital imaging together with the FUCCI cell cycle reporter, we identified that the G_1 arrest observed in SCC FAK-/- cells *in vivo* was overcome following IGFBP3 depletion (Figs. 3c and 3d). However, the defect in blood vessel formation was still evident in the SCC FAK-/- shRNA-IGFBP3 tumors as measured by the presence of CD31^{+} vessels (Figs. 3e and 3f). Therefore, IGFBP3 likely contributes to regulation of SCC tumor growth through controlling cell cycle progression, but not angiogenesis. Furthermore, depletion of IGFBP3 in SCC FAK-/- cells was not sufficient to fully restore tumor growth, implying that regulation of angiogenesis is likely also important.

FAK nuclear localization is required for regulation of IGFBP3 transcription

We have recently reported in SCC cells that nuclear FAK can bind to transcription factors and transcriptional regulators with the potential to influence gene expression (17). To investigate the requirement for FAK nuclear localization in regulation of *Igfbp3*, we made a series of FAK nuclear targeting mutants according to previously reported findings that identified putative nuclear localization sequences within the F2 lobe of the FERM domain (40), and expressed these in SCC FAK-/- cells. A total of three nuclear targeting mutants were constructed as follows: (1) by replacing arginine residues at positions 177 and 178 with alanines (FAK-177/178), (2) by replacing lysine residues at positions 190 and 191 with alanines (FAK-190/191), and (3) by replacing lysine residues at positions 216 and 218 with alanines (FAK-216/218). We have previously reported a fourth mutant deficient in nuclear targeting, in which all six of these amino acid residues have been replaced with alanines (17). Biochemical fractionation followed by western blotting was used to assess nuclear/cytoplasmic distribution of the resulting mutants when re-expressed in SCC FAK-/- cells, revealing that all four mutant FAK proteins were deficient in their ability to localize to the nucleus (Fig. 4a). Given that all of the double mutants appeared as defective in nuclear translocation as the mutant harboring all six mutations, we chose to move forward with these for further analysis. (q)RT-PCR analysis of *Igfbp3* expression in cell lines expressing these mutant FAK proteins revealed significantly increased levels of *Igfbp3* transcript in all three cell lines (Fig. 4b), implying a crucial role for FAK nuclear targeting in the transcriptional regulation of *Igfbp3*. The inability of these mutants to completely restore *Igfbp3* transcript levels to that of SCC FAK-/- cells is likely the consequence of low levels of residual nuclear FAK (Fig. 4a).

Runx1 is required for FAK-dependent transcriptional regulation of IGFBP3

To better define the link between nuclear FAK and regulation of *Igfbp3* transcription, we next sought to identify transcription factors with predicted binding sites in the promoter of the *Igfbp3* gene. Using the DECODE database (Qiagen), we generated a list of transcription factors predicted by text mining to bind between 20 kb upstream and 10 kb downstream of the human transcription start site (Fig. 4c). Of these transcription factors, three – Sp1, Runx1, and components of the transcription factor IID complex (TFIID) – were detected by mass spectrometry in a nuclear FAK interactome in SCC cells (Fig. 4c, dark grey bars) (17). We noted that the transcription factor Runx1, which has been reported to regulate *Igfbp3* gene expression (41), had the most *Igfbp3* promoter binding sites predicted by text mining (Fig. 4c). Moreover, Runx1 was not among the top transcription factors predicted to bind to the gene promoters of the other secreted proteins in the cluster highly upregulated in SCC FAK-/- conditioned medium (Supplementary Fig. 1, top cluster, and Supplementary Fig. 3), suggesting that these other angiogenesis-related proteins may be transcriptionally regulated by a distinct mechanism to *Igfbp3*.

Using shRNA-mediated stable knockdown of Runx1 expression, we next determined whether Runx1 was required for IGFBP3 expression in SCC FAK-wt and SCC FAK-/- cells. Biochemical fractionation followed by western blotting confirmed a substantial knockdown of Runx1 expression in both SCC FAK-wt shRNA-Runx1 and SCC FAK-/- shRNA-Runx1 cells (Fig. 4d) when compared to controls. Analysis of *Igfbp3* expression in these cell lines using (q)RT-PCR showed a loss of *Igfbp3* gene expression in SCC FAK-/- shRNA-Runx1 cells, reverting expression levels down to those observed in SCC FAK-wt vector-only control cells (Fig. 4e). Thus, Runx1 is required for increased *Igfbp3* transcription following FAK loss in SCC cells. Using an independent method of expression knockdown, similar results were observed following depletion of Runx1 using siRNAs (Supplementary Fig. 4).

FAK is in a complex with Runx1 in the nucleus

Analysis of Runx1 expression in SCC FAK-wt and FAK-/- cells revealed that Runx1 is exclusively expressed in the nucleus, and that its expression level is not regulated by FAK (Fig. 4d). Hence, regulation of Runx1 expression / degradation is unlikely the mechanism through which FAK controls Runx1 transcriptional activity in SCC cells. Runx1 can act as either a transcriptional activator or repressor, and the composition of the proteins interacting with Runx1 at a given gene can modulate this function (18). Using a mass spectrometry dataset of the nuclear FAK interactome in SCC cells (17) we identified a potential FAK / Runx1 interaction. Co-immunoprecipitation of Runx1 and FAK in SCC FAK-wt but not in SCC FAK-/- cells confirmed a novel association between FAK and Runx1 (Figs. 5a and 5b). Thus, nuclear FAK exists in complex with Runx1 under steady-state conditions in SCC cancer cells.

A key mechanism of Runx1 regulation is post-translational modification. Runx1 interacts with a number of proteins including kinases, histone acetyltransferases, arginine methyltransferases, and histone deacetylases that can post-translationally modify Runx1, switching it between transcriptional activation and repression (18,19). To further explore how FAK influences Runx1 function, we examined the Runx1 interaction landscape in the

context of FAK. To do this, we constructed a Runx1 protein interaction network *in silico*, onto which we mapped the experimentally derived nuclear FAK interactome. This integrated interaction network identified a subnetwork of Runx1 regulators and associated proteins that interact with FAK in the nuclei of SCC cells (Fig. 5c and Supplementary Fig. 5). Interestingly, a number of these proteins, including DNA (cytosine-5)-methyltransferase 1 (Dnmt1), Sin3a, Histone deacetylases 1, 2, and 3 (HDAC1, 2, and 3), and Nuclear receptor corepressor 1 and 2 (NCoR1 and 2), are linked to repression of Runx1 transcriptional activity (18,19). Therefore, nuclear FAK interacts with proteins that can regulate the post-translational modification and transcriptional function of Runx1. KEGG analysis also identified an enrichment for proteins with roles in the cell cycle (Fig. 5d and Supplementary Table 1), consistent with a complex that may play a wider role in the regulation of cell cycle progression.

To determine whether FAK regulated Runx1 tyrosine phosphorylation, we used immunoprecipitation of tyrosine phosphorylated proteins from SCC FAK-wt and FAK-/- cell lysates, followed by western blotting and detection with an anti-Runx1 antibody. No regulation of Runx1 tyrosine phosphorylation was observed (Fig. 5e). To assess Runx1 post-translational modification on a wider scale we performed 2D gel electrophoresis using nuclear extracts prepared from SCC FAK-wt and FAK-/- cells, and probed these gels with an anti-Runx1 antibody. This identified a number of potential differences in both the migration and intensity of spots detected (Fig. 5f, red arrows highlight changes), consistent with an altered state of post-translational modification.

We next investigated whether FAK regulated proteins associated with the post-translational modification of Runx1. Based on data presented in Fig. 5c, we focused on Sin3a, a transcriptional co-repressor known to interact with a number of HDACs (42) and suppress Runx1 transcriptional activity (43). Western blotting using an anti-Sin3a antibody identified reduced Sin3a levels in the nucleus of SCC FAK-/- cells when compared to SCC FAK-wt cells (Fig. 5g). Co-immunoprecipitation from SCC FAK-wt and FAK-/- nuclear extracts confirmed a novel association between Sin3a and FAK in SCC FAK-wt cells (Fig. 5h). Thus, FAK is in complex with and regulates the nuclear levels of a Sin3a. Immunoprecipitation of Runx1 from SCC FAK-wt and FAK-/- nuclear extracts followed by western blotting and detection with an anti-Sin3a antibody confirmed an association between Runx1 and Sin3a in SCC FAK-wt cells (Fig. 5i). No interaction was observed in SCC FAK-/- cells. Therefore, we propose that one potential mechanism through which FAK may influence the post-translational modification and transcriptional activity of Runx1, is through regulating the expression and subsequent recruitment of Sin3a to Runx1 transcriptional complexes.

Discussion

Numerous studies have demonstrated the importance of FAK in regulating tumor cell behavior, which has largely been linked to its role in integrating signals from adhesion sites and growth factor receptors at the cell periphery to control cell adhesion, migration and survival (1,2). In addition, it is now becoming clear that FAK can also play a role within the nucleus to control gene expression (14,17,44). However, the mechanisms underpinning this function remain to be fully characterized. A number of nuclear FAK binding proteins have

now been identified including the transcription factors p53 and GATA4 (14,16). Recently, we have shown that nuclear FAK is associated with chromatin and interacts with transcription factors, including the TBP-associated factor TAF9, and transcriptional regulators reported or predicted to regulate expression of the chemokine Ccl5. In doing so, it controls the transcription of chemokines that regulate the composition of the immuno-suppressive tumor environment required to evade the CD8^{+} T-cell anti-tumor immune response (17). Here, we identify a novel interaction between nuclear FAK and the transcription factor Runx1. We show that nuclear FAK controls the Runx1 dependent expression of IGFBP3, which in turn regulates cell cycle progression and SCC tumor growth *in vivo*. Further, we identify that FAK interacts with and regulates the nuclear levels of Sin3a, and that FAK is required for recruitment of Sin3a into complex with Runx1. Therefore, nuclear FAK can regulate transcription factor activity, potentially via recruitment of proteins to transcriptional complexes that can alter transcription factor post-translational modification, thereby controlling expression of specific genes that can play an important role in regulating both tumor cell behavior, and how tumor cells influence the composition of the tumor immune environment.

Runx1 is a transcription factor with an important role in both normal development and disease (20,21). De-regulation of Runx1 function contributes to the development of hematological malignances, and in solid epithelial cancers, it has been identified as both a tumor promoter and a tumor suppressor (19). Runx1 can either activate or repress transcription depending on the composition of the protein complexes with which it is associated at a given gene (18), and this likely contributes to the complexity of its role in regulating tumorigenesis. It is known to interact with an array of proteins including kinases, histone acetyltransferases, arginine methyltransferases, histone deacetylases, and ubiquitin ligases, all of which can post-translationally modify Runx1 to regulate its transcriptional function (18,19). Using mass spectrometry, we show that FAK interacts with a number of these proteins including Dnmt1, Sin3a, HDACs 1, 2, and 3, and NCoR1 and 2, all of which are known to repress Runx1 function (18,19). Co-immunoprecipitation experiments confirmed a novel interaction between Sin3a and FAK, and further identified a requirement for FAK to promote interaction of Runx1 with Sin3a. Supporting this as a potential mechanism of FAK-dependent Runx1 regulation, 2D gel analysis of nuclear extracts from SCC FAK-wt and FAK-/- cells using an anti-Runx1 antibody identified several protein species that show differential migration, consistent with altered post-translational modification. Notably, post-translational modification is an important mechanism in the general regulation of transcription factor function (45). Thus, we conclude that this may represent a previously unknown mode of FAK-dependent regulation of gene expression.

FAK is known to regulate a number of cellular processes important for the malignant phenotype (1,2). Here, we identify a new role for nuclear FAK in regulation of SCC cell cycle progression *in vivo* via controlling Runx1-dependent expression of IGFBP3. IGFBP3 has been linked to cell cycle arrest in tumor cells previously where a G1 arrest was accompanied by reduction in a number of cyclins, including cyclin D1, CDKs, and increased p21 expression (34,35). IGFBP3 has also been linked to regulation of angiogenesis (36–38). However, knockdown of IGFBP3 in the SCC cells had no effect on tumor angiogenesis. Analysis of secreted proteins present in SCC conditioned media identified a number of

changes including multiple factors that can influence tumor angiogenesis, implying that other factors may be more important in the regulation of angiogenesis in our SCC model. Interestingly, analysis of the predicted transcription factor binding sites in the promoters of other angiogenesis-related genes regulated by FAK identified that their mechanism of regulation is likely distinct to that of IGFBP3, highlighting the potential mechanistic diversity underpinning FAK-dependent transcriptional regulation.

The data presented here sheds new light on the possible mechanisms underpinning nuclear FAK-dependent regulation of gene expression, highlighting the importance of FAK as a scaffold for protein interactions in the nucleus. Future work should focus on FAK associated transcription factors to define how their interactome may change in the absence of FAK, or its kinase activity, and what the biological and potential clinical relevance of these changes may be.

Supplementary Material

Refer to Web version on PubMed Central for supplementary material.

Acknowledgments

Abbreviations

FAK	focal adhesion kinase
FERM	four-point-one, ezrin, radixin, moesin
FUCCI	fluorescent ubiquitination-based cell-cycle indicator
GFP	green fluorescent protein
IGFBP3	insulin-like growth factor binding protein 3
Runx1	Runt-related transcription factor 1
SCC	squamous cell carcinoma

References

1. McLean GW, Carragher NO, Avizienyte E, Evans J, Brunton VG, Frame MC. The role of focal-adhesion kinase in cancer - a new therapeutic opportunity. Nature reviews Cancer. 2005; 5:505–15. [PubMed: 16069815]

2. Sulzmaier FJ, Jean C, Schlaepfer DD. FAK in cancer: mechanistic findings and clinical applications. Nature reviews Cancer. 2014; 14:598–610. [PubMed: 25098269]

3. Ashton GH, Morton JP, Myant K, Phesse TJ, Ridgway RA, Marsh V, et al. Focal adhesion kinase is required for intestinal regeneration and tumorigenesis downstream of Wnt/c-Myc signaling. Developmental cell. 2010; 19:259–69. [PubMed: 20708588]

4. Lahlou H, Sanguin-Gendreau V, Zuo D, Cardiff RD, McLean GW, Frame MC, et al. Mammary epithelial-specific disruption of the focal adhesion kinase blocks mammary tumor progression. Proceedings of the National Academy of Sciences of the United States of America. 2007; 104:20302–7. [PubMed: 18056629]

5. Luo M, Fan H, Nagy T, Wei H, Wang C, Liu S, et al. Mammary epithelial-specific ablation of the focal adhesion kinase suppresses mammary tumorigenesis by affecting mammary cancer stem/progenitor cells. Cancer research. 2009; 69:466–74. [PubMed: 19147559]

6. McLean GW, Komiyama NH, Serrels B, Asano H, Reynolds L, Conti F, et al. Specific deletion of focal adhesion kinase suppresses tumor formation and blocks malignant progression. Genes Dev. 2004; 18:2998–3003. [PubMed: 15601818]

7. Provenzano PP, Inman DR, Eliceiri KW, Beggs HE, Keely PJ. Mammary epithelial-specific disruption of focal adhesion kinase retards tumor formation and metastasis in a transgenic mouse model of human breast cancer. The American journal of pathology. 2008; 173:1551–65. [PubMed: 18845837]

8. Pylayeva Y, Gillen KM, Gerald W, Beggs HE, Reichardt LF, Giancotti FG. Ras- and PI3K-dependent breast tumorigenesis in mice and humans requires focal adhesion kinase signaling. The Journal of clinical investigation. 2009; 119:252–66. [PubMed: 19147981]

9. Slack-Davis JK, Hershey ED, Theodorescu D, Frierson HF, Parsons JT. Differential requirement for focal adhesion kinase signaling in cancer progression in the transgenic adenocarcinoma of mouse prostate model. Molecular cancer therapeutics. 2009; 8:2470–7. [PubMed: 19671741]

10. Gabarra-Niecko V, Schaller MD, Dunty JM. FAK regulates biological processes important for the pathogenesis of cancer. Cancer metastasis reviews. 2003; 22:359–74. [PubMed: 12884911]

11. Siesser PM, Hanks SK. The signaling and biological implications of FAK overexpression in cancer. Clinical cancer research : an official journal of the American Association for Cancer Research. 2006; 12:3233–7. [PubMed: 16740741]

12. van Nimwegen MJ, van de Water B. Focal adhesion kinase: a potential target in cancer therapy. Biochemical pharmacology. 2007; 73:597–609. [PubMed: 16997283]

13. Lee BY, Timpson P, Horvath LG, Daly RJ. FAK signaling in human cancer as a target for therapeutics. Pharmacol Ther. 2015; 146:132–49. [PubMed: 25316657]

14. Lim ST, Chen XL, Lim Y, Hanson DA, Vo TT, Howerton K, et al. Nuclear FAK promotes cell proliferation and survival through FERM-enhanced p53 degradation. Mol Cell. 2008; 29:9–22. [PubMed: 18206965]

15. Ossovskaya V, Lim ST, Ota N, Schlaepfer DD, Ilic D. FAK nuclear export signal sequences. FEBS Lett. 2008; 582:2402–6. [PubMed: 18549812]

16. Lim ST, Miller NL, Chen XL, Tancioni I, Walsh CT, Lawson C, et al. Nuclear-localized focal adhesion kinase regulates inflammatory VCAM-1 expression. J Cell Biol. 2012; 197:907–19. [PubMed: 22734001]

17. Serrels A, Lund T, Serrels B, Byron A, McPherson RC, von Kriegsheim A, et al. Nuclear FAK controls chemokine transcription, Tregs, and evasion of anti-tumor immunity. Cell. 2015; 163:160–73. [PubMed: 26406376]

18. Brettingham-Moore KH, Taberlay PC, Holloway AF. Interplay between Transcription Factors and the Epigenome: Insight from the Role of RUNX1 in Leukemia. Front Immunol. 2015; 6:499. [PubMed: 26483790]

19. Goyama S, Huang G, Kurokawa M, Mulloy JC. Posttranslational modifications of RUNX1 as potential anticancer targets. Oncogene. 2015; 34:3483–92. [PubMed: 25263451]

20. Kurokawa M. AML1/Runx1 as a versatile regulator of hematopoiesis: regulation of its function and a role in adult hematopoiesis. Int J Hematol. 2006; 84:136–42. [PubMed: 16926135]

21. Okuda T, van Deursen J, Hiebert SW, Grosveld G, Downing JR. AML1, the target of multiple chromosomal translocations in human leukemia, is essential for normal fetal liver hematopoiesis. Cell. 1996; 84:321–30. [PubMed: 8565077]

22. Hoi CS, Lee SE, Lu SY, McDermitt DJ, Osorio KM, Piskun CM, et al. Runx1 directly promotes proliferation of hair follicle stem cells and epithelial tumor formation in mouse skin. Mol Cell Biol. 2010; 30:2518–36. [PubMed: 20308320]

23. Fijneman RJ, Anderson RA, Richards E, Liu J, Tijssen M, Meijer GA, et al. Runx1 is a tumor suppressor gene in the mouse gastrointestinal tract. Cancer Sci. 2012; 103:593–9. [PubMed: 22171576]

24. Serrels A, McLeod K, Canel M, Kinnaird A, Graham K, Frame MC, et al. The role of focal adhesion kinase catalytic activity on the proliferation and migration of squamous cell carcinoma cells. Int J Cancer. 2012; 131:287–97. [PubMed: 21823119]

25. de Hoon MJ, Imoto S, Nolan J, Miyano S. Open source clustering software. Bioinformatics. 2004; 20:1453–4. [PubMed: 14871861]

26. Saldanha AJ. Java Treeview--extensible visualization of microarray data. Bioinformatics. 2004; 20:3246–8. [PubMed: 15180930]

27. Shannon P, Markiel A, Ozier O, Baliga NS, Wang JT, Ramage D, et al. Cytoscape: a software environment for integrated models of biomolecular interaction networks. Genome Res. 2003; 13:2498–504. [PubMed: 14597658]

28. Huang da W, Sherman BT, Lempicki RA. Systematic and integrative analysis of large gene lists using DAVID bioinformatics resources. Nat Protoc. 2009; 4:44–57. [PubMed: 19131956]

29. Canel M, Serrels A, Miller D, Timpson P, Serrels B, Frame MC, et al. Quantitative in vivo imaging of the effects of inhibiting integrin signaling via Src and FAK on cancer cell movement: effects on E-cadherin dynamics. Cancer Res. 2010; 70:9413–22. [PubMed: 21045155]

30. Mitra SK, Mikolon D, Molina JE, Hsia DA, Hanson DA, Chi A, et al. Intrinsic FAK activity and Y925 phosphorylation facilitate an angiogenic switch in tumors. Oncogene. 2006; 25:5969–84. [PubMed: 16682956]

31. Sakaue-Sawano A, Kurokawa H, Morimura T, Hanyu A, Hama H, Osawa H, et al. Visualizing spatiotemporal dynamics of multicellular cell-cycle progression. Cell. 2008; 132:487–98. [PubMed: 18267078]

32. Jiang H, Hegde S, Knolhoff BL, Zhu Y, Herndon JM, Meyer MA, et al. Targeting focal adhesion kinase renders pancreatic cancers responsive to checkpoint immunotherapy. Nat Med. 2016; 22:851–60. [PubMed: 27376576]

33. Tavora B, Reynolds LE, Batista S, Demircioglu F, Fernandez I, Lechertier T, et al. Endothelial-cell FAK targeting sensitizes tumours to DNA-damaging therapy. Nature. 2014; 514:112–6. [PubMed: 25079333]

34. Kim HS, Lee WJ, Lee SW, Chae HW, Kim DH, Oh Y. Insulin-like growth factor binding protein-3 induces G1 cell cycle arrest with inhibition of cyclin-dependent kinase 2 and 4 in MCF-7 human breast cancer cells. Horm Metab Res. 2010; 42:165–72. [PubMed: 19960406]

35. Wu C, Liu X, Wang Y, Tian H, Xie Y, Li Q, et al. Insulin-like factor binding protein-3 promotes the G1 cell cycle arrest in several cancer cell lines. Gene. 2013; 512:127–33. [PubMed: 23041555]

36. Kim JH, Choi DS, Lee OH, Oh SH, Lippman SM, Lee HY. Antiangiogenic antitumor activities of IGFBP-3 are mediated by IGF-independent suppression of Erk1/2 activation and Egr-1-mediated transcriptional events. Blood. 2011; 118:2622–31. [PubMed: 21551235]

37. Liu B, Lee KW, Anzo M, Zhang B, Zi X, Tao Y, et al. Insulin-like growth factor-binding protein-3 inhibition of prostate cancer growth involves suppression of angiogenesis. Oncogene. 2007; 26:1811–9. [PubMed: 16983336]

38. Oh SH, Kim WY, Lee OH, Kang JH, Woo JK, Kim JH, et al. Insulin-like growth factor binding protein-3 suppresses vascular endothelial growth factor expression and tumor angiogenesis in head and neck squamous cell carcinoma. Cancer Sci. 2012; 103:1259–66. [PubMed: 22494072]

39. Baxter RC. IGF binding proteins in cancer: mechanistic and clinical insights. Nature reviews Cancer. 2014; 14:329–41. [PubMed: 24722429]

40. Brantley-Sieders DM, Zhuang G, Hicks D, Fang WB, Hwang Y, Cates JM, et al. The receptor tyrosine kinase EphA2 promotes mammary adenocarcinoma tumorigenesis and metastatic progression in mice by amplifying ErbB2 signaling. The Journal of clinical investigation. 2008; 118:64–78. [PubMed: 18079969]

41. Iwatsuki K, Tanaka K, Kaneko T, Kazama R, Okamoto S, Nakayama Y, et al. Runx1 promotes angiogenesis by downregulation of insulin-like growth factor-binding protein-3. Oncogene. 2005; 24:1129–37. [PubMed: 15592512]

42. Kadamb R, Mittal S, Bansal N, Batra H, Saluja D. Sin3: insight into its transcription regulatory functions. Eur J Cell Biol. 2013; 92:237–46. [PubMed: 24189169]

43. Zhao X, Jankovic V, Gural A, Huang G, Pardanani A, Menendez S, et al. Methylation of RUNX1 by PRMT1 abrogates SIN3A binding and potentiates its transcriptional activity. Genes Dev. 2008; 22:640–53. [PubMed: 18316480]

44. Lim ST. Nuclear FAK: a new mode of gene regulation from cellular adhesions. Molecules and cells. 2013

45. Filtz TM, Vogel WK, Leid M. Regulation of transcription factor activity by interconnected post-translational modifications. Trends Pharmacol Sci. 2014; 35:76–85. [PubMed: 24388790]
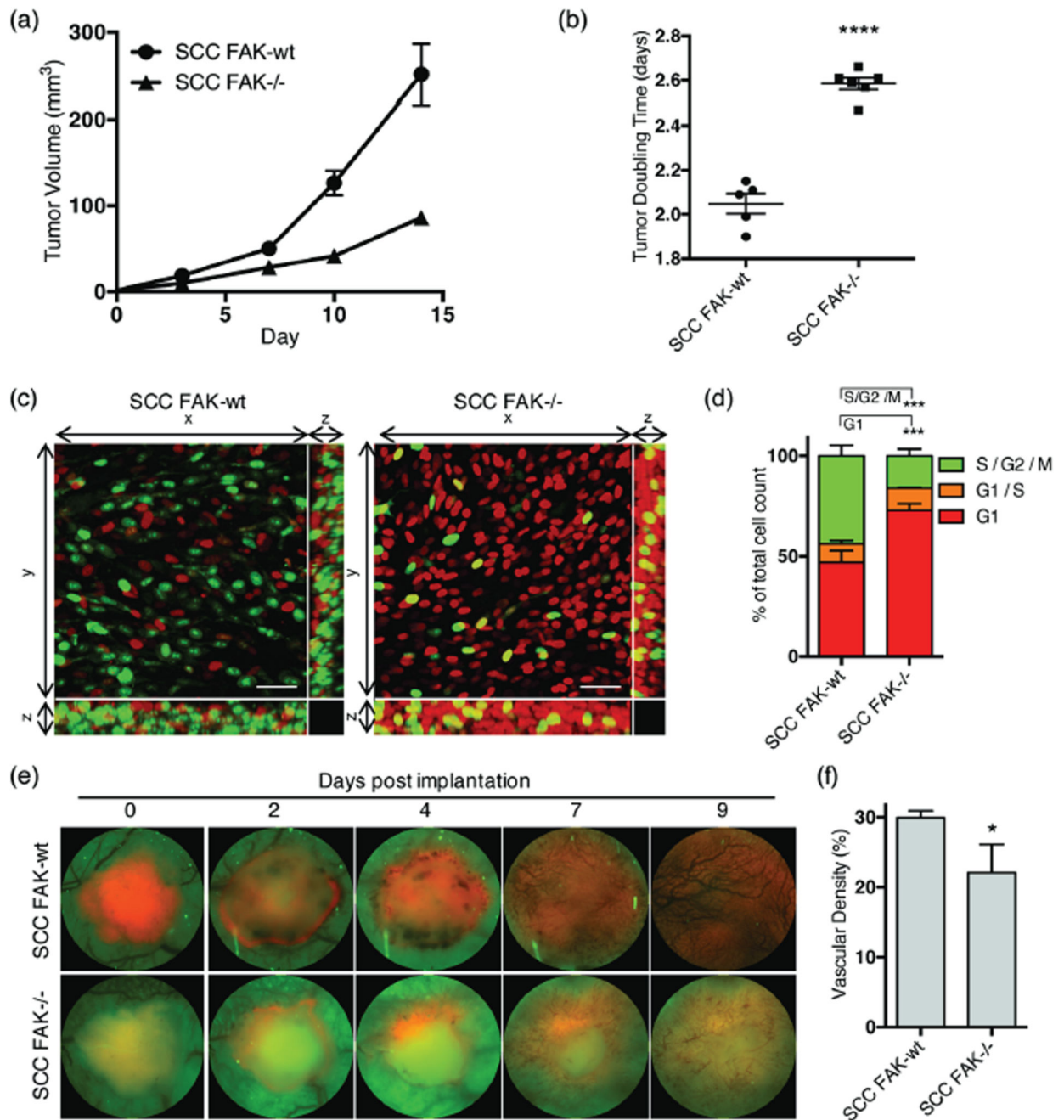
Figure 1. FAK regulates SCC tumor growth, cell cycle and angiogenesis *in vivo*.
(a) Growth of SCC FAK-wt and SCC FAK-/- tumor xenografts in CD-1 nude mice. n = 5 - 6 tumors per group. (b) SCC FAK-wt and SCC FAK-/- tumor doubling time. Unpaired T-test, ****p < 0.0001. (c) Intra-vital imaging of FUCCI expressing SCC FAK-wt and SCC FAK-/- cells 24 hours post-implantation under dorsal skinfold windows. (d) Quantitation of FUCCI cell cycle distribution from 3-dimentional image stacks shown in panel c. Sidak's corrected 2way ANOVA, ***p < 0.001. n = 4 tumors per group. (e) Longitudinal imaging of tumour angiogenesis following implantation of tumour fragments under dorsal skinfold windows.

Red – tagRFP labelled SCC tumor, Green – tissue autofluorescence. (f) Quantitation of blood vessel density at day 9. Unpaired T-test, *p = 0.0306. Data in all graphs represented as mean +/- s.e.m. n = 3 tumors per group.
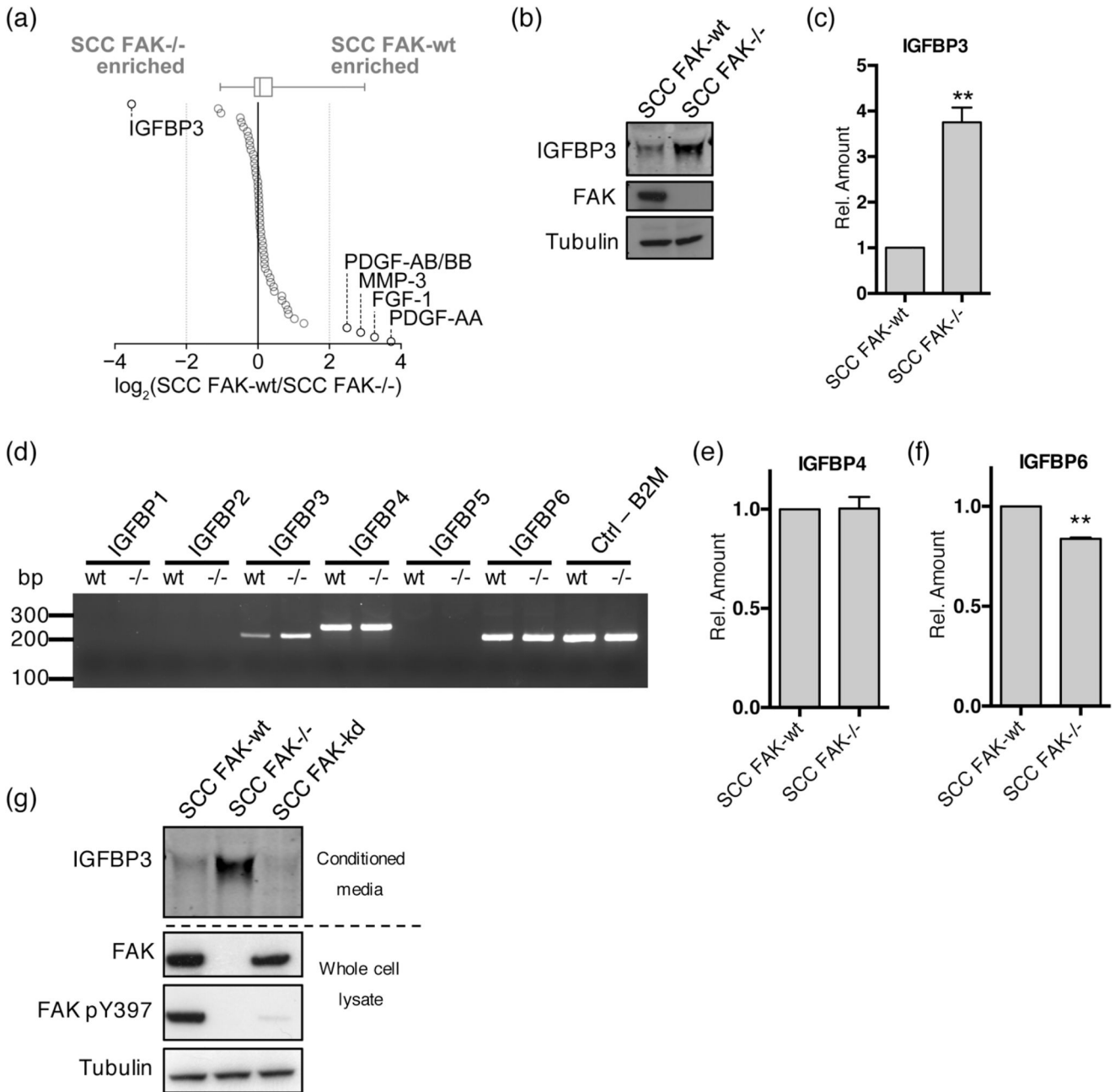
Figure 2. FAK negatively regulates the expression of IGFBP3 but not other IGFBP family members.

(a) Relative secreted levels of 53 angiogenesis-related proteins measured by antibody capture array from media conditioned by SCC FAK-wt and FAK-/- cells. Proteins are ordered by fold change. Dotted gray lines indicate four-fold enrichment; proteins changed by at least four fold are indicated. Box-and-whisker plot summarizes the median (line), 25th and 75th percentiles (box) and 5th and 95th percentiles (whiskers). (b) Representative anti-IGFBP3 western blot from concentrated conditioned media. (c) (q)RT-PCR analysis of IGFBP3 transcript levels in SCC FAK-wt and FAK-/- cells. n = 3. (d) Representative PCR

analysis of IGFBP family transcript levels in SCC FAK-wt and FAK-/- cells. (e) (q)RT-PCR analysis of IGFBP4 transcript levels in SCC FAK-wt and FAK-/- cells. n = 3. (f) (q)RT-PCR analysis of IGFBP6 transcript levels in SCC FAK-wt and FAK-/- cells. n = 3. (g) Representative anti-IGFBP3 western blot showing secreted IGFBP3 protein levels from SCC FAK-wt, SCC FAK-/-, and SCC FAK-kd cells. Data in all graphs represented as mean +/- s.e.m. Unpaired T-test, **p < 0.01.

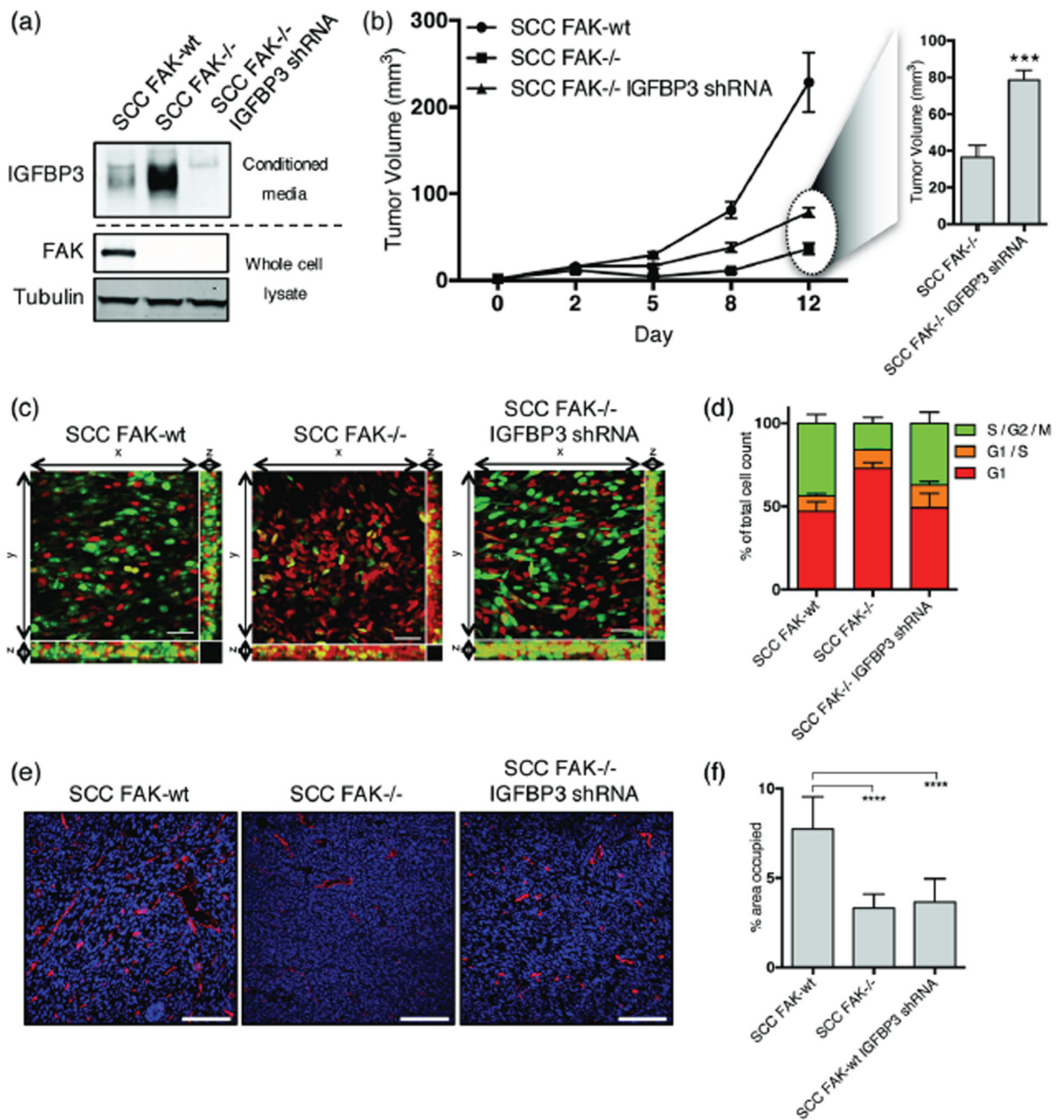**Figure 3. IGFBP3 regulates cell cycle progression but not tumor angiogenesis.**
(a) Representative anti-IGFBP3 western blot from concentrated media conditioned by either
SCC FAK-wt, SCC FAK-/-, or SCC FAK-/- IGFBP3 shRNA cells. Anti-FAK western blot
shows FAK expression status and Anti-tubulin western blot was used a loading control. (b)
Left - Growth of SCC FAK-wt, SCC FAK-/-, and SCC FAK-/- IGFBP3 shRNA tumor
xenografts in CD-1 nude mice. *Right* – Average volume of SCC FAK-/- and SCC FAK-/-
IGFBP3 shRNA tumors at day 12. Unpaired T-test, ***$p < 0.001$. n = 6 tumors per group.
(c) Intra-vital imaging of FUCCI expressing SCC FAK-wt, SCC FAK-/-, and SCC FAK-/-

IGFBP3 shRNA cells 24 hours post-implantation under dorsal skinfold windows. (d) Quantitation of FUCCI cell cycle distribution from 3-dimentional image stacks shown in panel c. Values shown for SCC FAK-wt and SCC FAK-/- cells are repeated from Fig. 1d. n = 4 tumors per group. (e) Fluorescent staining of frozen tissue sections using anti-CD31 antibody (red). Nuclei labelled using DAPI (blue). (f) Quantitation of the % area occupied by CD31$^+$ cells. Tukey's corrected one-way ANOVA, ****p < 0.0001. Data in all graphs represented as mean +/- s.e.m. n = 3 tumors per group with an average of 3 fields measured per tumor.
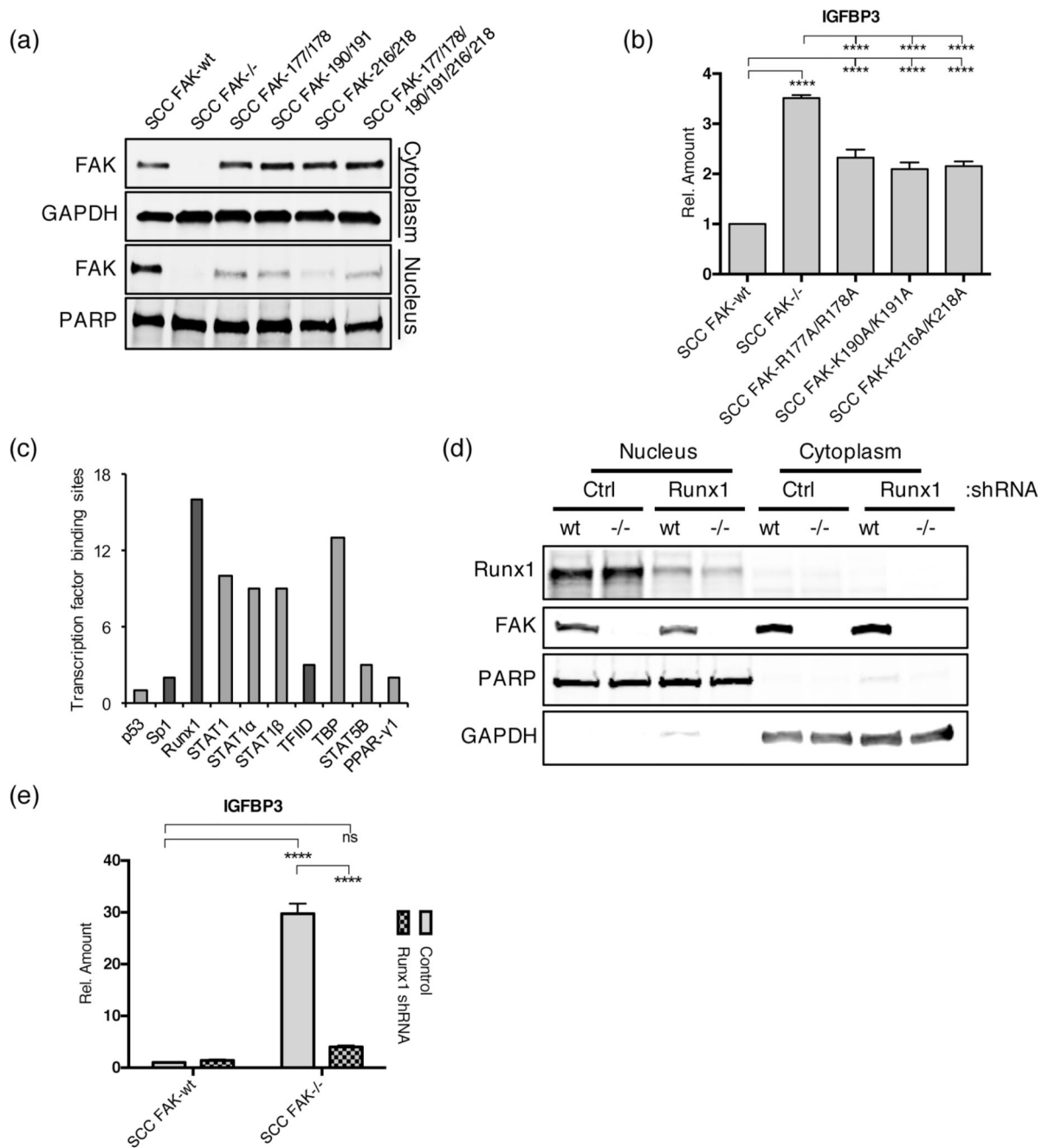
Figure 4. Nuclear FAK and RUNX1 regulate IGFBP3 expression.
(a) Representative anti-FAK western blot of cytoplasmic and nuclear fractions prepared from a series of SCC cells expressing FAK nuclear localization signal (NLS) mutants. (b) (q)RT-PCR analysis of IGFBP3 expression in SCC cells expressing FAK NLS mutants. Tukey's corrected 1way ANOVA, ****p < 0.0001. Data in all graphs represented as mean +/- s.e.m. n = 3. (c) Predicted transcription factor binding sites in the promoter of *Igfbp3*. Transcription factors that interact with nuclear FAK in SCC cells are displayed in dark grey. (d) Representative western blot showing Runx1 depletion using shRNA. (e) (q)RT-PCR analysis

of IGFBP3 expression in control and Runx1 depleted SCC FAK-wt and SCC FAK-/- cells. Sidak's corrected 2way ANOVA, ****$p < 0.0001$. ns = not significant. n = 3.
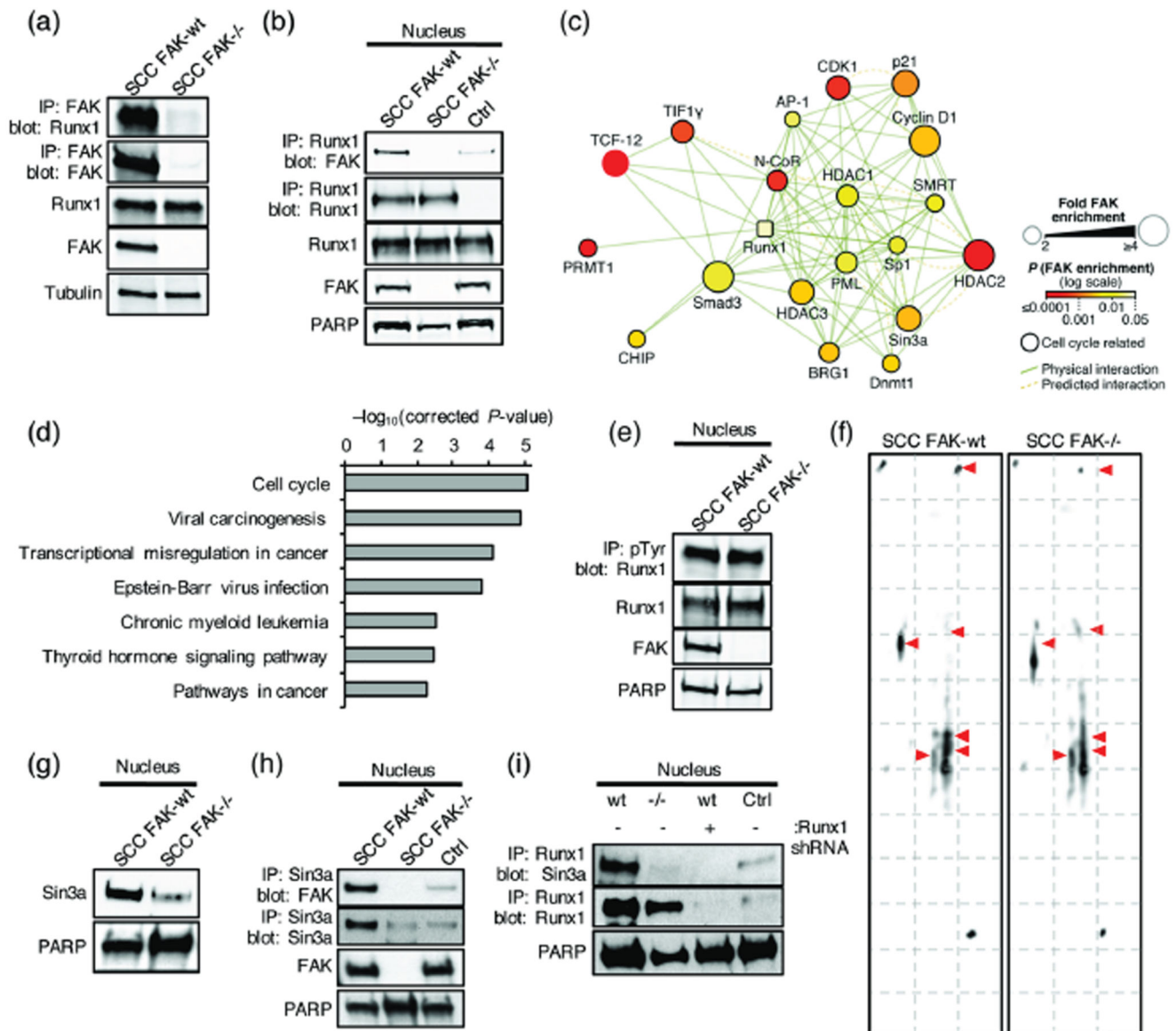
Figure 5. Nuclear FAK interacts with Runx1.

(a) Representative western blot of anti-FAK immunoprecipitation probed with anti-Runx1 antibody. (b) Representative western blot of anti-Runx1 immunoprecipitation probed with anti-FAK antibody. IgG control (Ctrl). (c) Interaction network analysis of physical or predicted direct binders of Runx1 that interact with FAK in the nucleus of SCC cells (see Supplementary Table 2). Runx1 is shown as a square node. Protein node size is proportional to fold enrichment in nuclear FAK immunoprecipitations. Node color indicates significance of enrichment in nuclear FAK immunoprecipitations. (d) Pathway enrichment analysis of KEGG terms in the nuclear FAK interactome of Runx1 binders ($Q < 0.01$) (see Supplementary Fig. 5). (e) Representative western blot of anti-phospho-tyrosine (pTyr) immunoprecipitation probed with anti-Runx1 antibody. (f) 2D gel electrophoresis probed with anti-Runx1 antibody. (g) Representative western blot of SCC FAK-wt and FAK-/-

nuclear lysates probed with anti-Sin3a antibody. (h) Western blot of anti-Sin3a immunoprecipitation from SCC FAK-wt and FAK-/- nuclear lysates probed with anti-FAK antibody. IgG control (Ctrl) was done using SCC FAK-wt nuclear lysates. (i) Western blot of anti-Runx1 immunoprecipitation from SCC FAK-wt, SCC FAK-/-, and SCC FAK-wt Runx1 shRNA nuclear lysates probed with anti-Sin3a antibody. IgG control (Ctrl) was done using SCC FAK-wt nuclear lysates.